ACS APPLIED MATERIALS & INTERFACES

Research Article

Cite This: ACS Appl. Mater. Interfaces 2019, 11, 11976−11987

www.acsami.org

Design, Synthesis, and Evaluation of CF_3AuCNR Precursors for Focused Electron Beam-Induced Deposition of Gold

Will G. Carden,[†] Rachel M. Thorman,[‡,§] Ilyas Unlu,[‡,§] Khalil A. Abboud,[†] D. Howard Fairbrother,[‡] and Lisa McElwee-White*[,†]

[†]Department of Chemistry, University of Florida, Gainesville, Florida 32611-7200, United States

[‡]Department of Chemistry, Johns Hopkins University, Baltimore, Maryland 21218-2685, United States

Supporting Information

ABSTRACT: The Au(I) complexes $CF_3AuCNMe$ (**1a**) and CF_3AuCN^tBu (**1b**) were investigated as Au(I) precursors for focused electron beam-induced deposition (FEBID) of metallic gold. Both **1a** and **1b** are sufficiently volatile for sublimation at 125 ± 1 mTorr in the temperature range of roughly 40−50 °C. Electron impact mass spectra of **1a**−**b** show gold-containing ions resulting from fragmenting the CF_3 group and the CNR ligand, whereas in negative chemical ionization of **1a**−**b**, the major fragment results from dealkylation of the CNR ligand. Steady-state depositions from **1a** in an Auger spectrometer produce deposits with a similar gold content to the commercial precursor $Me_2Au(acac)$ (**3**) deposited under the same conditions, while the gold content from **1b** is less. These results enable us to suggest the likely fate of the CF_3 and CNR ligands during FEBID.

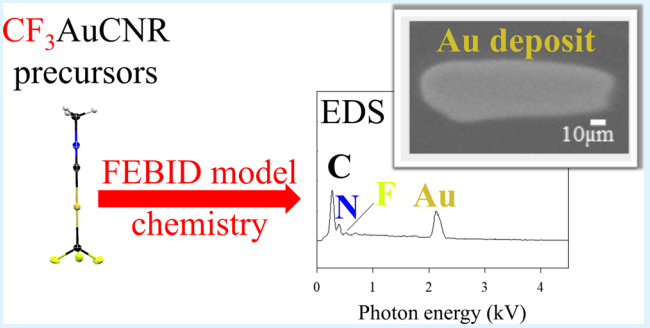

KEYWORDS: *Au(I) precursors, mechanism based precursor design, focused electron beam-induced deposition, gold plasmonic structures, aurophilic interactions*

INTRODUCTION

Early work in the field of plasmonics is over 100 years old;[1] however, the field has more recently seen dramatic growth following the 1998 observation by Ebbesen of extraordinarily high optical transmission efficiencies through subwavelength holes in metallic films because of the coupling of the incident light with surface plasmons.[2] In the intervening 20 years since this discovery, plasmonics has gained relevance in a wide variety of fields, from surface-enhanced Raman spectroscopy, which utilizes localized plasmon resonances generated in metallic nanoscale structures to detect single molecules, to biosensing and optoelectronics.[3] As plasmonics can be used to "break the diffraction limit" of optical devices, the miniaturization of plasmonic structures to the nanoscale has gained considerable importance.[3,4] Noble metals, such as gold, are popular materials out of which to make plasmonic nanostructures,[3,4] due to their negative dielectric permittivity at optical frequencies and high conductivity.[5] Plasmonic applications require these metallic nanostructures to have high purity and well-defined structures to display optimal optical properties with minimal losses.[6] However, traditional nanolithography methods can produce nanostructures with contamination from resists or ion implantation, as well as surface roughness from sputtered metal films.[7−9]

Unlike traditional top-down approaches, focused electron beam-induced deposition (FEBID) is a maskless, vacuum-based, resistless bottom-up nanofabrication method capable of directly writing three-dimensional metal-containing nanostructures onto nonplanar surfaces.[8,9] In FEBID, a focused electron beam impinges upon a substrate that is exposed to a volatile organometallic complex. Electron-driven reactions cause the organometallic precursor to decompose in a spatially localized area defined by the primary electron beam, depositing metal-containing fragments on the substrate, while other volatile fragments desorb into the vacuum.

Commercially available chemical vapor deposition (CVD) precursors such as dimethylgold(III) acetylacetonate ($Me_2Au(acac)$),[10−13] dimethylgold(III) trifluoroacetylacetonate ($Me_2Au(tfac)$),[13,14] and dimethylgold(III) hexafluoroacetylacetonate ($Me_2Au(hfac)$)[15] have historically been used as gold precursors in FEBID. However, such precursors are optimized for thermally induced decomposition, rather than electron-induced decomposition. In addition, coreactants are commonly used in CVD and their presence may be required for decomposition. Because of the different decomposition pathways under CVD and FEBID conditions, FEBID deposits made from CVD precursors are typically plagued by low metal content because of the presence of organic contamination that

Received: October 21, 2018
Accepted: March 5, 2019
Published: March 5, 2019

Downloaded via UNIV OF FLORIDA on September 10, 2021 at 19:47:03 (UTC).
See https://pubs.acs.org/sharingguidelines for options on how to legitimately share published articles.

© 2019 American Chemical Society

DOI: 10.1021/acsami.8b18368
ACS Appl. Mater. Interfaces 2019, 11, 11976−11987

originates from the incomplete desorption and/or decomposition of the ligands. In the cases of $Me_2Au(acac)$, $Me_2Au(tfac)$, and $Me_2Au(hfac)$, the reported metal contents of gold deposits produced by FEBID have been 3−40 at. % Au,[10,11,16−19] 8−40 at. % Au,[14,16,17,20,21] and 2−3 at. % Au,[15] respectively. This variability arises from the differences in the deposition conditions and the means of analyzing the deposits. Although the atomic percentage of gold in these deposits is commonly higher than that of the precursor molecule, significantly higher purity nanostructures are required for plasmonic applications.[14,17,22]

To improve the gold content of nanostructures deposited using FEBID, several different avenues have been explored. These can be roughly categorized into three areas: postdeposition purification, in situ deposit purification, and precursor choice. The most common method of postdeposition purification is annealing, which can in the case of gold deposits improve nanostructure purity from an initial ∼40 at. % Au to a purity of 82 at. % Au after annealing at 400 °C in air.[23] Annealing may also be performed under a reactive atmosphere, such as oxygen[19] or ozone,[17] improving nanostructure purities, for example, from an initial 8 at. % Au to 60 at. % Au[19] and from an initial ∼20 at. % Au to pure Au nanostructures,[17] respectively. Although postdeposition annealing can produce high-purity Au nanostructures from commercially available CVD precursors, it does have some drawbacks—annealing under a reactive ozone atmosphere produced a 2−3 times reduced volume of the nanostructure,[17] and significant morphology changes are common upon annealing.[8] As plasmonic applications require precise definition in nanostructure morphology, the use of postdeposition annealing for purification of FEBID nanostructures may severely limit their plasmonic application. Postdeposition oxygen plasma treatment is another promising purification method.[18] However, it still produces significantly reduced volume of the as-deposited nanostructures.[18]

Deposit purification in situ can take several forms. Deposition onto a heated substrate improved the purity of gold nanostructures deposited from $Me_2Au(acac)$ from an initial ∼18 at. % Au to a final purity of 30 at. % Au; however, deposition yield decreased sharply with temperature, and at higher temperatures (>120 °C), thermal decomposition began to be competitive with FEBID. Further, this purification method requires the use of a specialized heated stage. Another in situ deposition method of producing high-purity gold nanostructures is deposition under a reactive atmosphere of water, which has resulted in 91 at. % Au from $Me_2Au(tfac)$.[14]

The most direct method to improve Au content in FEBID deposits is to tailor the Au-containing precursors. To this end, there have also been efforts to look beyond the Au(III) CVD precursors for complexes to be used in Au FEBID. The most successful of these involved chloro(trifluorophosphine)gold(I) ($ClAuPF_3$) and chloro(carbonyl)gold(I) (ClAuCO), which produced highly pure Au deposits by FEBID.[24−27] Deposits made from $ClAuPF_3$ had a resistivity of 22 $\mu\Omega$ cm (10 times that of bulk gold),[28] and deposits made from ClAuCO were greater than 95 at. % Au.[27] Despite the high purity and low resistivity of their deposits, these compounds are considered undesirable as FEBID precursors because of their lability toward thermal decomposition and sensitivity to air and water.[13,27,28] Several gold compounds with relatively low carbon content, $[ClAuMe_2]_2$, $ClAuSMe_2$, $ClAuPMe_3$, and $MeAuPMe_3$, were also recently prescreened for possible viability as FEBID precursors.[13] While $ClAuSMe_2$ and $ClAuPMe_3$ were found unsuitable because they decompose before volatilization, $[ClAuMe_2]_2$ and $MeAuPMe_3$ were found to produce deposits with 29−41 at. % Au and 19−25 at. % Au, respectively.[13]

In this study, we report the design and synthesis of two organometallic gold(I) complexes, $CF_3AuCNMe$ (**1a**)[29] and CF_3AuCN^tBu (**1b**),[30] along with their characterization and prescreening as FEBID precursors. Gold-containing structures deposited from these precursors were compared with deposits made from the commercially available CVD precursor $Me_2Au(acac)$ (**3**) in the same system and under similar deposition conditions. Compositional analysis of deposits formed using the two organometallic gold(I) complexes via electron-induced deposition under ultrahigh vacuum (UHV) conditions provides additional insight into the elementary reactions that underpin FEBID.

EXPERIMENTAL SECTION

General Procedures. *Synthesis.* All synthetic manipulations were carried out under a dinitrogen atmosphere using standard Schlenk and glovebox techniques. Glassware was flame-dried before use. Diethylether (Et_2O) and tetrahydrofuran (THF) were distilled over sodium benzophenone and stored over activated 3 Å molecular sieves. Acetonitrile (CH_3CN) was purified using an MBraun MB-SP solvent purification system and stored over activated 3 Å molecular sieves. Methylene chloride (HPLC grade), hexanes (ACS grade), and pentane (HPLC grade) were purchased from either Fisher Scientific or Sigma-Aldrich and used as received. Trifluoromethyl-(trimethylsilane), 99%, was purchased from Sigma-Aldrich and degassed by three freeze−pump−thaw cycles prior to use. Silver(I) fluoride was purchased from either Alfa Aesar or Oakwood Chemical and used as received. Chloro(dimethylsulfide)gold(I) was purchased from either Sigma-Aldrich or Oakwood Chemical and used without further purification. *tert*-Butyl isocyanide, 98% was purchased from Sigma-Aldrich and used as received. Methyl isocyanide[31] and ClAuCNR complexes (**2a** and **2b**)[32] were prepared as previously described and characterized by comparison to literature data. Chloroform-d_1 was purchased from Cambridge Isotope Laboratories, Inc. and stored over activated 3 Å molecular sieves (15%, w/v) on the bench top. All NMR experiments were conducted using an Inova 500 MHz spectrometer. Infrared spectra were acquired with a PerkinElmer Spectrum One Fourier transform infrared spectrometer.

*$CF_3AuCNMe$ (**1a**).* This procedure was adapted from a literature method[30] for the synthesis of other CF_3AuL complexes. The compound was identified by comparison to literature data.[29] A Schlenk flask was charged with AgF (521.3 mg, 4.109 mmol) in an N_2-filled glovebox. The flask was moved to a Schlenk line where dry THF (24 mL) was added to suspend AgF. Degassed CF_3TMS (2.0 mL, 14 mmol) was added, and the suspension was stirred in the absence of light at room temperature for 30 min. In a subsequent step, **2a** (740.3 mg, 2.707 mmol) was added to the flask and the reaction mixture was stirred in the absence of light for 24 h. The volatiles were then removed under reduced pressure, and the product was extracted with methylene chloride. The filtrate was filtered over CH_2Cl_2-rinsed Celite and concentrated under vacuum. Addition of pentane and storage at −20 °C led to crystallization. The colorless needles were isolated by washing with −20 °C pentane to afford 357.1 mg (43% yield) of the pure product. Although compound **1a** has been reported, its characterization was incomplete. ^1H NMR (500 MHz, $CDCl_3$, 25 °C): δ 3.41 ppm (t, 3H, $^2J_{HN}$ = 2.5 Hz); ^{13}C NMR (126 MHz, $CDCl_3$, 25 °C): δ 155.82 ppm (qt, CF_3, $^1J_{CF}$ = 341.0 Hz, $^3J_{CN}$ = 3.4 Hz), 146.97 (m, C≡N) ppm, 29.34 ppm (t, CH_3, $^1J_{CN}$ = 8.7 Hz); ^{19}F NMR (470 MHz, $CDCl_3$, 25 °C): δ −28.71 ppm (s, 3F); FTIR (ATR) ν_{CN} 2283 cm^{-1}, ν_{CF} 1119 cm^{-1}, ν_{CF} 983 cm^{-1}.

*CF_3AuCN^tBu (**1b**).* This procedure was adapted from a literature method,[30] and the compound was characterized by comparison to literature data.[30,33] A Schlenk flask was charged with AgF (504.8 mg,

DOI: 10.1021/acsami.8b18368
ACS Appl. Mater. Interfaces 2019, 11, 11976−11987

3.979 mmol) in an N_2-filled glovebox. The flask was moved to a Schlenk line where dry Et_2O (24 mL) was added to suspend AgF. Degassed CF_3TMS (1.9 mL, 13 mmol) was added, and the suspension was stirred in the absence of light at room temperature for 1 h. In a subsequent step, **2b** (789.9 mg, 2.503 mmol) was added to the flask and the reaction mixture was stirred in the absence of light for 48 h. The volatiles were then removed under reduced pressure, and the crude product was extracted with methylene chloride using a Celite plug. The colorless filtrate was brought to dryness under vacuum and dry-loaded onto a silica gel (Dynamic Adsorbents Inc., 60 Å, 32−63 μm) column. The pure product was eluted with 50% CH_2Cl_2/hexanes via flash chromatography to give 343.2 mg (39% yield) of white solid. ^{1}H NMR (500 MHz, $CDCl_3$, 25 °C): δ 1.57 ppm (s, 9H). ^{13}C NMR (126 MHz, $CDCl_3$, 25 °C): δ 156.13 (q, CF_3, $^1J_{CF}$ = 341.6 Hz), 145.13 ppm (m, C≡N), 59.11 ppm (s, N−C), 29.82 ppm (s, CH_3). ^{19}F NMR (470 MHz, $CDCl_3$, 25 °C): δ −28.74 ppm. FTIR (ATR): ν_{CN} 2245 cm^{-1}, ν_{CF} 1125 cm^{-1}, ν_{CF} 984 cm^{-1}.

Mass Spectrometry. Mass spectra were collected using a Thermo Scientific DSQ II instrument equipped with a Thermo Scientific direct insertion probe (DIP) and a controller operating at a base pressure on the order of 10^{-7} Torr. DIP-electron ionization (DIPEI) experiments utilized a 70 eV ion source maintained at 60 ± 7 °C during operation. Once the sample was evacuated, the probe was held at 30 °C for 10 s and ramped to 60 °C at a rate of 60 °C/min and held for 10 min. Similar conditions were used for DIP-negative chemical ionization (DIPNCI) experiments. Data reduction was carried out using Qual Browser, Thermo Xcalibur 2.2 SP1.48, August 12, 2011.

Determination of Sublimation Temperature. Sublimation experiments were carried out using the procedures and equipment described previously.[34] All compounds were purified (vide supra) and ground into fine powders prior to use. Compounds **1a** and **1b** (45.0 mg each) were loaded individually into flame-dried Schlenk flasks equipped with a drip-tip cold finger and set up on a pressure-controlled Schlenk line. A recirculating chiller was connected in series, and each cold finger was cooled to 8 °C. Each flask was submerged in a silicone oil bath and then simultaneously opened to dynamic vacuum (125 ± 1 mTorr). The hot plates were simultaneously ramped from room temperature at a rate of 15 °C every 30 min until sublimation was noted. The onset of sublimation was marked by the temperature of the oil bath at which a white film was observed on the cold finger. All sublimation experiments were allowed to proceed overnight, and the purity of each sublimate was ascertained by ^{1}H and ^{19}F NMR.

Determination of Decomposition Temperature. These experiments were conducted under ambient conditions with no attempts to exclude oxygen or moisture. Compounds **1a** and **1b** were loaded into individual melting point capillaries (single opening) and heated side-by-side in a melting point apparatus equipped with an oil bath. The decomposition temperature (at 760 Torr) was noted as the temperature of the oil when discoloration was observed.

Vacuum-Based Studies. *General.* Deposition and UHV surface science studies were performed on $CF_3AuCNMe$ (**1a**), CF_3AuCN^tBu (**1b**), and the commercially available precursor $Me_2Au(acac)$ (**3**) (CAS 14951-50-9, Strem Chemicals, Inc.). An UHV chamber equipped with an Auger electron spectrometer (AES) was used to make gold structures from **1a**, **1b**, and **3** using electron-beam irradiation under a constant supply of precursor. The second UHV chamber containing an X-ray photoelectron spectrometer and a quadrupole mass spectrometer was used to study the electron-induced reactions of adsorbed **1a** under precursor-limited conditions. More detailed discussions of each of these instruments have been published previously.[35,36]

The procedure for introducing compounds into both UHV chambers was essentially identical for each precursor. First, the precursor in question was added to a glass finger attached to a UHV-compatible precision leak valve. This was carried out in a glovebox under an inert N_2 atmosphere. The glass finger/leak valve combination was then attached directly to the respective UHV chamber.

Deposition Experiments. The base pressure of the UHV chamber housing the Auger spectrometer was approximately 2−4 × 10^{-9} Torr for all experiments. A silicon substrate, generated by sputtering with 4 keV Ar^+ ions to remove the native oxide layer and adventitious carbon, was used for all depositions. The surface composition was determined using a PHI 610 Scanning Auger Microprobe system (LaB_6 filament), which was also used as a primary electron beam for electron-induced deposition of the precursors. The substrate was maintained at room temperature during all depositions.

Precursors **1a** and **1b** were heated to 60 °C to increase their vapor pressures, while precursor **3** was sufficiently volatile at room temperature. The precursors were then introduced to the chamber through a UHV-compatible precision leak valve and onto the substrate through a directional doser, the latter being a 0.125″ diameter stainless steel tube placed about 1 cm from the sample surface at an angle of 45° with respect to the plane of the surface. We estimate that this leads to a local pressure enhancement of approximately tenfold as compared to the background pressure as measured by the ion gauge. During deposition, the background pressure of precursor molecules was 5 × 10^{-9} (precursor **1a**), 8 × 10^{-9} (precursor **1b**), and 3 × 10^{-8} (precursor **3**) Torr. Assuming an average base pressure of 3 × 10^{-9} Torr (i.e., in the absence of precursor deposition), this yields molecular fluxes of 2.4 × 10^{12}, 5.6 × 10^{12}, and 3.0 × 10^{13} molecules cm^{-2} s^{-1} for precursor **1a**, precursor **1b**, and precursor **3**, respectively. Deposits were made under steady-state conditions under a constant partial pressure of precursor molecules and using a primary electron-beam energy of 3 kV and a target current of approximately 1 μA. During deposition, the electron beam was not rastered and its shape and location on the substrate surface remained invariant. Because the size of the deposits is determined by that of the electron gun (vide infra), this beam current corresponds to an electron flux of ≈1.33 × 10^{17} electrons s^{-1} cm^{-2}. Although this target current is significantly greater than the nA current typically reported in FEBID studies, the size of the deposits being made is also considerably larger. As a result, the flux of electrons is comparable to values used in FEBID, and we do not expect there to be any significant increases in the local temperature in the irradiated region during deposition (Supporting Information, page S-16).

Depositions from **1a** and **1b** lasted for 24 h, while depositions from **3** required 4 h. Deposits were then characterized in situ using AES and ex situ using a cold-cathode field-emission scanning electron microscopy (SEM, JEOL 6700F, resolution of 1.0 nm, primary beam energy of 10 kV for imaging) equipped with energy-dispersive spectrometry (EDS) (EDAX Genesis 4000 X-ray analysis system, resolution of 129 eV, primary beam energy of 5 kV for EDS). EDS quantification was conducted in the absence of any standards, although we note that using the same instrument, we have recently determined that deposits created from $Pt(CO)_2Cl_2$ exhibited a Pt/Cl stoichiometry of 1:2 in accord with the stoichiometry of the compound and the predictions of separate UHV surface science studies.[37]

Electron-Induced Reactions of 1a. An UHV chamber equipped with an X-ray photoelectron spectrometer, mass spectrometer, and a flood gun electron source had a base pressure of approximately 2 × 10^{-9} Torr. Highly ordered pyrolytic graphite (HOPG) and gold were used as substrates. Prior to adsorbing nanometer-scale films of **1a**, substrates were cleaned by sputtering with 4 keV Ar^+ ions, with surface cleanliness verified by an X-ray photoelectron spectrometer.

Thin films of $CF_3AuCNMe$ (**1a**) were produced by subliming the precursor at 65 °C and leaking it into the chamber through a UHV-compatible precision leak valve to produce a chamber pressure of 5−6 × 10^{-9} Torr. The gas was adsorbed onto a cooled 1 cm^2 substrate held at 125 ± 5 K. Films were subsequently exposed to 500 eV electrons using a commercial flood gun source (Spec FG 15/40). The thin films studied in an X-ray photoelectron spectrometer were exposed to longer exposure times at a fixed target current of 5 μA/3.13 × 10^{13} electrons s^{-1} cm^{-2}. A Phi 5400 X-ray photoelectron spectrometer in Mg anode (Mg Kα X-rays, $h\nu$ = 1254.6 eV) was used to characterize the substrate and adsorbed films before and after electron irradiation.

DOI: 10.1021/acsami.8b18368
ACS Appl. Mater. Interfaces 2019, 11, 11976−11987

RESULTS AND DISCUSSION

Precursor Design. In general, there are two goals in precursor design for FEBID: (1) minimize the number of atoms in the ligands, so that there is less material available to cause contamination in the deposits and (2) ensure sufficient thermal stability and volatility for transport in a gas injection system (GIS). A starting point for considering the precursor structure is the literature on FEBID from the Au(I) complexes $ClAuPF_3$ and ClAuCO. Both produce virtually pure gold deposits,[24−28] yet their practical use is limited by their thermal lability and air and water sensitivity.[38−41] Gold(I) complexes provide an interesting framework for FEBID precursors because their preference for being two-coordinate[42] minimizes the number of ligands that must be removed by electron-induced reactions to deposit pure metal. In comparison, the gold(III) precursors $Me_2Au(acac)$, $Me_2Au(tfac)$, and $Me_2Au(hfac)$ are four-coordinate. The thermal lability of $ClAuPF_3$ and ClAuCO is largely due to the low bond strength of Au(I) to the strong π-acid ligands CO and PF_3.[43] Bonding of metal centers to π-acids relies heavily on metal d→ligand π^* backbonding.[42] Despite its filled d shell, the large electronegativity and ionization potential of Au(I) make Au→L backbonding negligible, and, as a result, the Au−L bond is thermally labile in ClAuCO and $ClAuPF_3$. Ligand stability is also problematic for L = PF_3 as the ligand itself is water-sensitive.

Owing to the practical requirements for volatilization and transport through a GIS without decomposition, Au(I) complexes of the type XAuL (X = anionic ligand and L = neutral, two-electron donor ligand) with different L-type ligands have been investigated as potential precursors, with the goal of increasing thermal stability and volatility. Because the backbonding of Au(I) is poor, the thermal stability of XAuL complexes could be improved by increasing the σ-donor strength of the neutral ligand L. Neutral ligands such as trialkylphosphines and dialkylsulfides, which are better σ-donors than CO and PF_3, form XAuL complexes with increased thermal stability over the CO and PF_3 derivatives (Figure 1). Although complexes such as $ClAuSMe_2$ and

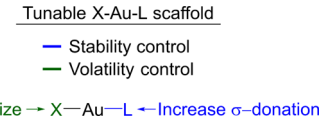

Figure 1. Tuning XAuL complexes for increased stability and volatility.

$ClAuPMe_3$ are sufficiently stable for standard storage and handling, they are not volatile enough for practical use.[13] As an alternative, we sought ligands that were isoelectronic with CO, a ligand that has been demonstrated to desorb under FEBID conditions.[37,44] Isocyanides were chosen for investigation because they are not only isoelectronic with the CO ligand, but are also stronger σ-donors relative to CO and PF_3, which will increase the stability of the complexes.

As FEBID takes place under high vacuum conditions in an electron microscope, precursor volatility is a critical consideration for practical applications and has been problematic for complexes of the type ClAuL.[13] However, in a recent study on the relative volatilities of XAuL complexes where X = Cl, Br, and I, the volatilities of the iodide complexes were consistently the highest in the series.[34] This effect was attributed to decreased aurophilic (Au−Au) bonding in the molecular lattice of the precursor. A reasonable design strategy would therefore be to vary the anionic X ligand in XAuL complexes as a means of controlling volatility in these complexes (Figure 1). In addition to the halide series, other possible anionic ligands include alkyl or fluoroalkyl groups. A similar investigation has shown that the gold alkyl CH_3AuPMe_3 has increased volatility over the chloride complex $ClAuPMe_3$ because of decreased Au−Au bonding imposed by the CH_3 group.[13,45] Additional volatility can be obtained by fluorination of ligands, a common strategy in the design of CVD precursors.[46] Thus, replacing the halide in XAuL complexes with a trifluoromethyl group will provide enhanced volatility. Although precursors containing alkyl groups (M−CH_3) have been studied in FEBID, the effects of the trifluoromethyl ligand are unknown.

These considerations led us to target the trifluoromethyl alkylisocyanide complexes $CF_3AuCNMe$ (**1a**) and CF_3AuCN^tBu (**1b**) as potential FEBID precursors. The combination of the strong σ-donor isocyanide ligands and the fluorinated alkyl was chosen to increase complex stability and volatility over the previously studied XAuL complexes such as ClAuCO, $ClAuPF_3$, $ClAuSMe_2$, and $ClAuPMe_3$.

Synthesis of Trifluoromethyl Au(I)CNR Complexes. The trifluromethyl gold complexes $CF_3AuCNMe$ (**1a**) and CF_3AuCN^tBu (**1b**) are easily accessed from the corresponding chloride complexes **2a** and **2b** (Scheme 1). Trifluoromethylation of **2a** and **2b** is carried out by transmetallation from $AgCF_3$, which is generated in situ from the reaction of CF_3TMS with AgF. This route has been previously published for **1b**,[30] but the literature preparation of **1a** utilizes the toxic, explosive, and pyrophoric[47] cadmium reagent $(CF_3)_2Cd$ as the transmetallation reagent.[29] In contrast, synthesis of **1a** via the Scheme 1 route is straightforward and avoids use of the cadmium reagent. Despite previous reports suggesting the formation of $AgCF_3$ is negligible in THF and Et_2O because of the low solubility of AgF,[48] our yields of **1a** in these solvents are similar to those obtained in the more commonly used CH_3CN. Both **1a** and **1b** can be stored at −20 °C indefinitely.

Scheme 1. Synthesis of Trifluoromethyl Gold Isocyanide Complexes 1a and 1b

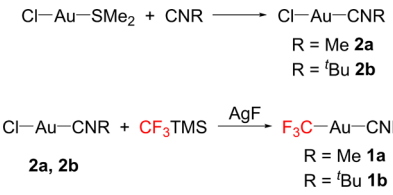

Precursor Volatility and Thermal Stability. Traditional FEBID experiments require gas-phase precursor transport from a crucible in the GIS to the substrate, which is located in a high-vacuum environment ($P < 10^{-5}$ Torr). Thus, precursors must be sufficiently volatile and thermally stable for successful transport and delivery. As a surrogate for vapor pressure measurements, we quantify precursor volatility through sublimation experiments carried out on a modified Schlenk line equipped with a pressure controller. When evaluating the data from these experiments, we understand that molecules travel shorter distances in our sublimators than they do in a GIS. We can, however, compare the behavior of new precursors in our sublimation experiments to the behavior of precursors known to be sufficiently volatile for use in a GIS.

DOI: 10.1021/acsami.8b18368
ACS Appl. Mater. Interfaces 2019, 11, 11976−11987

The sublimation experiments are conducted by heating an evacuated sublimator charged with the precursor in an oil bath at a constant rate. The sublimation onset temperature (T_{sub}) is noted as the temperature of the oil well at which the appearance of a white coating on the cold finger (cooled to 8 °C) is first detected. The constant pressure (125 ± 1 mTorr) provided by the pressure controller along with parallel sublimation of **1a** and **1b** ensures that reproducible values can be obtained for the temperatures and pressures necessary to volatilize and transport each compound in the gas phase. The T_{sub} values for **1a** and **1b** are shown in Table 1. After transport by sublimation, we assess the purity of the condensed sublimate through multinuclear NMR experiments. Thus, these experiments allow us to not only assess volatility but also to verify that the compounds are sufficiently stable to survive the transport process.

Table 1. Sublimation Onset Temperature (T_{sub}) and Decomposition Onset Temperature (T_d) for 1a, 1b, 2a, and 2b

precursor	T_{sub} (°C) at 125 ± 1 mTorr[a]	T_d (°C) at 1 atm[a]
$CF_3AuCNMe$ (**1a**)	51	80
CF_3AuCN^tBu (**1b**)	39	126
ClAuCNMe (**2a**)[b]	83	184
$ClAuCN^tBu$ (**2b**)[b]	64	162

[a]All temperature values are ±0.5 °C. [b]T_{sub} and T_d values are from ref 34.

As an additional measure of thermal stability, we determine the decomposition onset temperatures (T_d) of precursor candidates (Table 1) by heating the precursor in a melting point capillary at atmospheric pressure and observing discoloration of the precursor sample. Like the sublimation experiments, the decomposition temperatures are obtained by heating multiple precursors side-by-side for an accurate comparison.

For the trifluoromethyl complexes **1a** and **1b**, the sublimation onset temperature decreases as the steric bulk of the alkyl substituent of the isocyanide increases. Also, for each isocyanide, the trifluoromethyl complexes have lower sublimation temperatures than the respective chloride complexes. Attempts to observe sublimation at atmospheric pressure through thermogravimetric analysis (TGA) were unsuccessful because of decomposition or competing sublimation and decomposition (Figures S8 and S9).

Because the observed decomposition temperatures of **1a** and **1b** are higher than their sublimation temperatures, it should be possible to volatilize the precursors and transport them in the gas phase without significant decomposition. This is supported by the collection of white products on the cold finger during the sublimation of both **1a** and **1b** and the subsequent NMR characterization of each product. It is worth noting, however, that some decomposition occurs in the unsublimed portions of **1a** and **1b**, as noted by the appearance of gold plating or a pinkish hue. Although the trifluoromethyl complexes **1a** and **1b** have a lower onset decomposition temperature than the chloride complexes **2a** and **2b**, their decomposition temperatures are well above those of ClAuCO and $ClAuPF_3$, which decompose at room temperature and 40−45 °C, respectively.[13,41,49] The relatively low sublimation onset temperatures and moderate thermal stability of **1a** and **1b** prompted further study of their electron-induced reactivity.

Solid-State Structures of 1a and 1b. Single crystals of compound **1a** suitable for X-ray diffraction analysis were grown by the slow diffusion of pentane into a CH_2Cl_2 solution of the compound at −20 °C (Table 2). The solid-state structure of **1a** with relevant bond lengths and angles is shown in Figure 2, and its extended packing is depicted in Figure 3. Although the X-ray structure of compound **1b** has been reported,[30] its extended Au−Au bonding and packing were not provided. Thus, we report the solid-state structure and packing diagram for compound **1b** in Figure 4.

Table 2. Crystallographic Details for Compound 1a[a]

	1a
formula	$C_3H_3AuF_3N$
FW	307.03
crystal system	monoclinic
space group	$C2/m$
a (Å)	17.1992(12)
b (Å)	5.8322(4)
c (Å)	5.6685(4)
α (deg)	90
β (deg)	98.9460(10)
γ (deg)	90
volume (Å^3)	561.69(7)
Z	4
D_{calcd} (Mg/m^3)	3.631
total reflns	12 460
unique reflns	1167
GOF (S)	1.256
R_1, wR_2 [$I > 2\sigma(I)$]	0.0105, 0.0265 [1149]
R_1, wR_2 (all data)	0.0108, 0.0265

[a]$S = [\sum[w(F_o^2 - F_c^2)^2]/(n-p)]^{1/2}$. $R_1 = \sum(||F_o| - |F_c||)/\sum|F_o|$. $wR_2 = [\sum[w(F_o^2 - F_c^2)^2]/\sum[w(F_o^2)^2]]^{1/2}$. $w = 1/[\sigma^2(F_o^2) + (m \times p)^2 + n \times p]$, $p = [\max(F_o^2,0) + 2 \times F_c^2]/3$, m & n are constants.

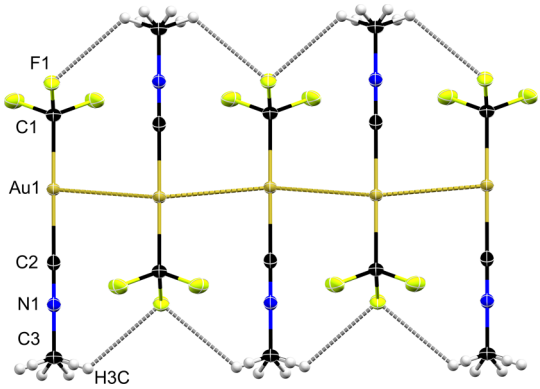

Figure 2. Solid-state structure of compound **1a** along the b-axis with ellipsoids drawn at 50% probability. Aurophilic interactions and H-bonding are shown (gold and gray dotted lines). Disorder in the H atoms is shown. Au1−C1 2.047(3) Å, Au1−C2 1.988(3) Å, Au1−Au1′ 3.4361(2) Å, Cu1−Au1−C2 175.74(11)°, and C1−Au1−Au1′−C1′ 180.00(0)°.

Compound **1a**, $CF_3AuCNMe$, crystallizes in the monoclinic space group $C2/m$ with similar unit-cell parameters to the isomeric acetonitrile complex $CF_3AuNCMe$ (Table 2).[33] In the molecular structure of **1a**, gold adopts a pseudolinear geometry (Figure 2). The linearity of the molecule extends

DOI: 10.1021/acsami.8b18368
ACS Appl. Mater. Interfaces 2019, 11, 11976−11987

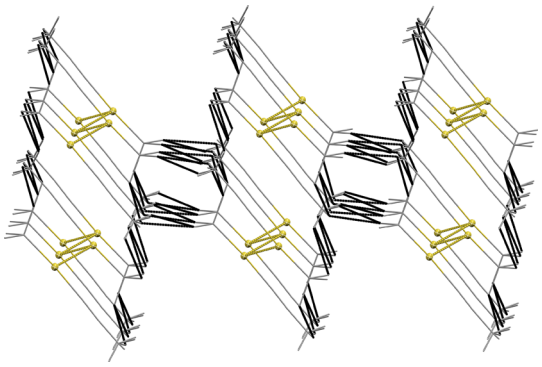

Figure 3. Molecular packing of compound **1a** viewed down the *b*-axis. Selected atoms are depicted in wireframe for clarity. Aurophilic interactions and H-bonding are shown (gold and black dotted lines).

throughout the entire C−Au−CNC linkage, which is consistent with other X−Au−CNR species. The Au−C1 bond length of 2.047(3) Å is similar to that found in other trifluoromethyl gold complexes, specifically CF_3AuCO (2.047(14) Å),[50] CF_3AuPPh_3 (2.045(4) Å),[51] CF_3AuPMe_3 (2.070(8), 2.056(8), and 2.062(9) Å),[30] and CF_3AuCN^tBu (2.034(3) and 2.031(4) Å).[30] The lengthening of the Au−C1 bond in **1a** compared to that found in the isomeric complex, $CF_3AuNCMe$ (2.002(8) Å),[33] is likely the result of a stronger trans-influence induced by the methylisocyanide ligand. Likewise, the Au−C2 distance of 1.988(3) Å is in good agreement with similar gold(I) isocyanides, namely, CF_3AuCN^tBu (1.988(4) and 1.996(4) Å),[30] ClAuCNMe (1.95(2) Å),[52] CNAuCNMe (1.98(5) Å),[53] $XAuCN^tBu$ (X = Cl 1.92(1),[54] Br 1.939(8),[30] and I 1.95(1) Å[55]), XAuCNCy (X = Cl 1.961(14), Br 1.972(7), and I 1.953(14) Å),[56] and ClAuCNAd (1.948(13) Å).[57]

In the lattice of **1a**, the $CF_3AuCNMe$ monomers are arranged in an antiparallel fashion, forming a polymeric zigzag chain of gold atoms that spans the length of the *b*-axis (Figures 2 and 3). The Au−Au distance along the chain (3.4361(2) Å) is shorter than the sum of two van der Waals radii for gold (3.7 Å)[58] and therefore suggestive of long aurophilic interactions. This distance is longer than that of **1b** which forms dimers at a Au−Au distance of 3.1526(2) Å. This is likely due to the larger steric demand of the *tert*-butyl group, which forces a smaller X−Au−Au′−X′ torsion angle relative to the methyl complex in order to maintain its Au−Au interaction. As an effect of the antiparallel juxtaposition of neighboring XAuL monomers in **1a**, a network of C−H···F interactions each with an H−F distance of 2.66 Å is formed along the *b*-axis (Figure 2). Other C−H···F interactions in **1a** are present but appear to connect adjacent sheets of polymeric chains rather than spanning the Au−Au chain itself like the former set (Figure S10). These involve slightly shorter H−F distances of 2.41, 2.59, and 2.60 Å (Table S5). Because the hydrogen atoms are located in geometrically idealized positions, the error range of the distance cannot be determined. Although C−H···F interactions are a nonclassical form of hydrogen bonding, several studies show that this type of interactions is not negligible, albeit weaker than classical hydrogen bonding[59,60] It has been shown that these interactions, when present, influence molecular packing in the solid state.[61] Owing to the smaller X−Au−Au′−X′ torsion angle in **1b**[30] (122.9(1)° compared to 180.00(0)° in **1a**), significantly less H-bonding is present in **1b** (2 H-bonds per two Au atoms in **1b** compared to 8 H-bonds per one Au atom in **1a**). This suggests that molecules are packed more efficiently in **1a** than in **1b**. The isomeric acetonitrile complex $CF_3AuNCMe$ forms a similar network of hydrogen bonds throughout the solid lattice, which likely arises from the same antiparallel arrangement of XAuL monomers as found in **1a**.[33]

Structural Effects on Volatility. Precursor volatility is largely controlled by the intermolecular interactions induced from lattice packing.[34] Generally speaking, the larger the average separation between molecules within the lattice (loose packing), the more volatile the precursor. Because aurophilic interactions have a significant effect on the solid-state packing of Au(I) precursors, analysis of these interactions in the solid-state structures can provide insight into the volatility trends.[34] The methyl isocyanide complex $CF_3AuCNMe$ (**1a**) crystallizes with a polymeric chain of Au atoms due to aurophilic interactions, while CF_3AuCN^tBu (**1b**) crystallizes in small, dimeric Au−Au aggregates, and as a result, T_{sub} is lower for **1b**. It can also be anticipated that intermolecular hydrogen bonding, which is energetically similar to Au−Au bonding,[58] influences precursor volatility. Thus, the larger number of hydrogen bonds present in **1a** causes its T_{sub} value to be higher than that of **1b**, despite the longer individual Au−Au bonds in **1a**.

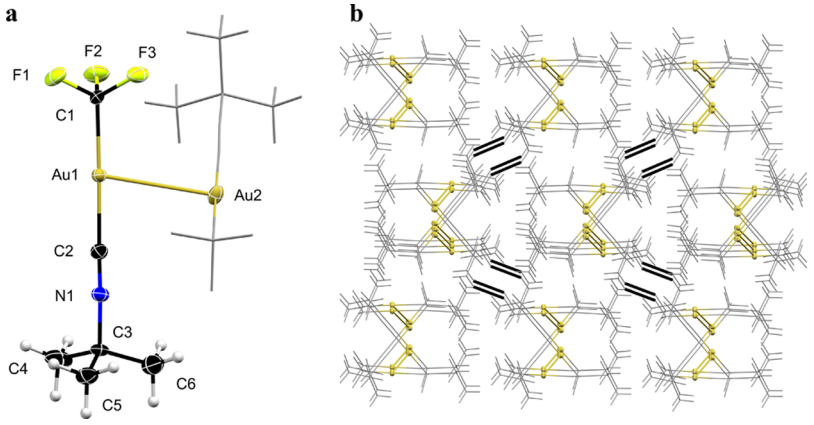

Figure 4. (a) Solid-state structure of a dimer of compound **1b**. Thermal ellipsoids are drawn at the 50% probability level. Selected atoms are depicted in a wireframe for clarity. Disorder in the CF_3 group is omitted for clarity. (b) Molecular packing of compound **1b** viewed down the *c*-axis. Selected atoms are depicted in a wireframe for clarity. Aurophilic interactions and H-bonding are shown (gold and black bonds).

DOI: 10.1021/acsami.8b18368
ACS Appl. Mater. Interfaces 2019, 11, 11976−11987

In comparing CF_3 complexes **1a**–**b** to the previously studied chloride complexes **2a**–**b**, the methylisocyanide complexes **1a** and **2a** display similar aurophilic bonding; both compounds align head to tail forming a 1D polymeric chain of gold atoms.[52] Although the polymeric chain of Au atoms in the trifluoromethyl complex **1a** consists of shorter Au–Au bonds than the polymeric chain in the chloride complex **2a** (3.4361(2) Å compared to 3.637(1) Å),[52] T_{sub} is lower for **1a** (Table 1). This result is attributed to the tighter crystal packing in **2a** compared to **1a** (Figure S11), which arises from the increased size and increased electronegativity of CF_3 relative to Cl.

When compared to the chloride complex **2b**, the trifluoromethyl derivative **1b** exhibits much shorter Au–Au interactions (3.1526(2) Å relative to 3.695(1) Å). However, the trifluoromethyl complex forms much more discrete dimeric aggregates compared to the polymeric chains in the lattice of the chloride complex, thus **1b** has a lower T_{sub} than **2b** (Table 1).

DIP Mass Spectrometry. Mass spectrometry (MS) has been widely used to gain insight into decomposition of precursors for thermal deposition techniques (CVD and ALD) and to do rapid prescreening of potential precursors to select candidates for more extensive deposition studies.[62] Despite the obvious differences between ionization and thermal decomposition, related intermediates are often observed in MS and pyrolysis experiments, which are collectively used for mechanism-based precursor design.[46] The following MS studies were carried out to explore the possibility of using a similar rapid precursor prescreening strategy for FEBID. Although we do not expect gas-phase MS experiments to be a perfect predictor of the electron-induced gas-surface reactions in FEBID, there is a value in developing a quick, easy, and inexpensive method for synthetic labs to downselect from the large variety of known complexes of a target metal to a small set of reasonable possibilities before the precursors are used in deposition experiments that are time-consuming and expensive. Fragmentation pathways observed in a gas-phase electron-impact mass spectrometer can provide an indication that similar pathways might be possible on a surface in FEBID and that the complex should be investigated further. The possibility of eventually developing a practical screening process based on MS makes it of interest to compare MS results to deposition results for both new and known precursors.

To simulate volatilization and gas-phase precursor transport in FEBID, a DIP was used to introduce the sample for all MS experiments. The DIP operates by heating the solid precursor under vacuum to volatilize the sample and introduce it into the ion source block. The abundant ions generated from DIP-electron impact (DIPEI) and DIP-NCI-MS (DIPNCI) MS of **1a**–**b** (Figures S15–S18) are summarized in Table 3 with alkyl isocyanide fragmentation from DIPEI-MS shown in Table S19.

In the EI experiments, extensive fragmentation is observed for both compounds as expected (Table 3), but **1b** displays significantly more fragmentation at the isocyanide ligand itself, consistent with a larger alkyl chain on the CNR backbone (Table S19). For both compounds, the molecular ion is detected with an appreciable abundance and there is no evidence for higher nuclearity fragments (dimer, trimer, and oligomer) up to the scan width of m/z = 1000, which suggests that the Au–Au bonds and hydrogen bonding networks present in the solid state are broken prior to the molecule reaching the gas phase. The same is true for both **1a** and **1b** in NCI.

Table 3. Selected Ions and Their Relative Abundances as Observed in Positive Ion DIPEI-MS and DIPNCI-MS of Compounds 1a and 1b[a]

EI ions	m/z (**1a**)	abundance (**1a**)[b]	m/z (**1b**)	abundance (**1b**)[c,d]
$[M]^{\bullet+}$	306.9	34	348.9	29
$[M - F]^+$	287.9	33	330.0	7
$[M - CF_3]^+$	238.0	100	280.0	53
$[AuCNCH_2]^+$	237.0	17	n.o.[e]	n.o.[e]
$[AuCNCH]^+$	236.0	5	n.o.[e]	n.o.[e]
$[CF_2AuCN + H]^+$	n.o.[e]	n.o.[e]	273.9	31
$[AuCNC(CH_3)_2]^+$	n.o.[e]	n.o.[e]	265.0	8
$[CF_2Au]^+$	n.o.[e]	n.o.[e]	246.9	8
$[AuCN + H]^+$	n.o.[e]	n.o.[e]	223.9	100
Au^+	196.9	16	196.9	5
$[CNR]^+$	41.1	10	n.o.[e]	n.o.[e]
$[CF_3]^+$	69.0	8	69.1	10
NCI ions	m/z (**1a**)	abundance (**1a**)[f]	m/z (**1b**)	abundance (**1b**)[g]
$[M - H]^-$	305.8	7	n.o.[e]	n.o.[e]
$[CF_3AuCN]^-$	291.8	100	291.7	100

[a]Relative abundances ≥ 5% are included. [b]Normalized to 238.0 m/z for **1a**. [c]Normalized to 223.9 m/z for **1b**. [d]CNR-derived fragments are listed in Table S19. [e]n.o. = not observed. [f]Normalized to 291.8 m/z for **1a**. [g]Normalized to 291.7 m/z for **1b**.

In EI, loss of CF_3 after ionization to generate the $[M - CF_3]^+$ species is common to both **1a** and **1b** (base peak for **1a**) and the concomitant formation of $[CF_3]^+$ is also observed for both. Fluorine loss resulting in $[M - F]^+$ fragments also occurs, but these species are less abundant than $[M - CF_3]^+$ ions. Net loss of one fluorine and the CNR ligand after ionization to form $[CF_2Au]^+$ occurs for **1b**, but not for **1a**. Other gold-containing ions contain fragments of the alkyl isocyanide ligand. For example, loss of one or two methyl hydrogens and the CF_3 group from **1a** produces $[AuCNCH_2]^+$ and $[AuCNCH]^+$, respectively. A similar fragment for **1b** corresponds to the loss of one methyl group along with CF_3 loss giving $[AuCNC(CH_3)_2]^+$. Additional methyl loss is not observed. Another fragment generated from CF_3^- loss from **1b** also includes loss of isobutylene to give $[AuCN + H]^+$. Additional fragmentation at the alkyl isocyanide is observed in ions containing incomplete dissociation of the CF_3 group. Net loss of fluorine and isobutylene from $M^{+\bullet}$ generates $[CF_2AuCN + H]^+$ for **1b**, but this fragment is absent in the mass spectrum of **1a**, presumably because of the difficulty of losing a methyl group by a related process. Although fragments corresponding to the loss of multiple fluorines (i.e., $[M - 2F]^+$ or $[M - 3F]^+$) were insignificant (<5% rel. abundance), $[CFAuCN]^+$ is observed for **1b**. Gold ions, Au^+, are observed for both compounds.

In NCI, less fragmentation is observed for **1a**–**b**, consistent with CI utilizing soft ionization relative to EI (Table 3). In lieu of the molecular ion for **1a**, there was a low-intensity signal from loss of one hydrogen, as expected for an *N*-methyl group. Common to both **1a** and **1b** is the dealkylation of the isocyanide to give $[CF_3AuCN]^-$ which is the base peak for both compounds and the only significant ion observed for **1b**. Fragmentation at the CF_3 group is not observed in NCI.

Deposition Experiments under UHV Conditions. To determine their potential utility in FEBID, CF_3AuCN^tBu (**1b**)

DOI: 10.1021/acsami.8b18368
ACS Appl. Mater. Interfaces 2019, 11, 11976–11987

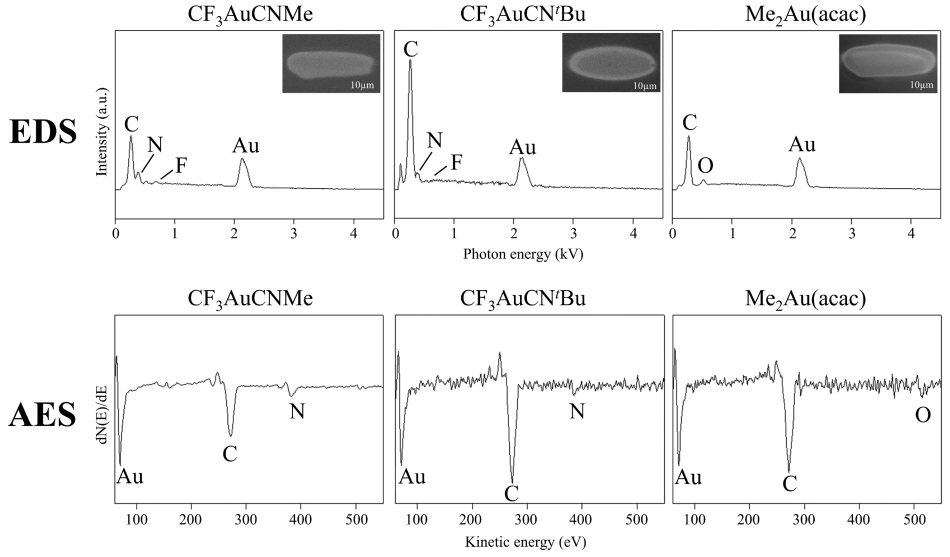

Figure 5. SEM, EDS, and AES data for deposits created from $CF_3AuCNMe$, CF_3AuCN^tBu, and $Me_2Au(acac)$ in an AES on a silicon substrate under steady-state conditions. SEM images of each deposit are shown as an inset within the respective EDS spectrum. Each EDS and AES spectrum is normalized to the Au peak to allow easy comparison.

Table 4. Atomic Percentages of Au, C, O, N, and F as Determined by EDS in Deposits from Figure 5[a]

precursor	at. % Au	at. % C	at. % O	at. % N	at. % F	C/Au (deposit)	C/Au (precursor)
$CF_3AuCNMe$ (**1a**)	22	62	<1%	14	0.9	2.8	3
CF_3AuCN^tBu (**1b**)	14	80	<1%	6	0	5.7	6
$Me_2Au(acac)$ (**3**)	25	72	3	n.o.[b]	n.o.[b]	2.9	7

[a]Carbon-to-gold ratios in the deposit and precursor are also included. [b]n.o. = not observed.

and $CF_3AuCNMe$ (**1a**) were used to produce gold-containing deposits in an Auger spectrometer ($P_{base} \approx 5 \times 10^{-9}$ Torr). The commercial precursor $Me_2Au(acac)$ (**3**) was used to provide a point of comparison to the two synthesized Au precursors. Figure 5 shows SEM, EDS, and AES data for deposits produced from **1b**, **1a**, and (**3**) on a silicon substrate. All three deposits were "spot deposits", spatially defined by the electron beam (whose shape and location on the substrate remained constant during deposition). The absence of any deposits or deposition outside of the region defined by the electron beam indicates that the deposits were formed as a result of electron beam-induced deposition; thus, they have the potential to serve as FEBID precursors. The Au peak area was normalized for each precursor in both the EDS and AES spectra to facilitate comparison of the differences in chemical composition. All three precursors produced deposits containing gold and carbon (Figure 5). Oxygen is also observed in the deposits created from $Me_2Au(acac)$. In contrast, nitrogen is observed in the deposits created from **1b** and **1a**, along with an extremely small fluorine signal (≤1%).

The elemental compositions of the three deposits determined by EDS are shown in Table 4. The EDS data were used to determine each deposit's composition as their thicknesses are greater than 100 nm, based on the absence of substrate peaks in EDS. Thus, EDS data reflect the overall composition of each deposit, while AES only measures the composition within the topmost surface layers (2−5 nm approximately). We chose to use the EDS data not only because it provided a more representative measure of deposit composition but also because the chemical composition determined by AES was far less reproducible than EDS (Figure S19). Based on the elemental compositions, the at. % Au obtained from $Me_2Au(acac)$ (25%) and $CF_3AuCNMe$ (22%) was similar, while the at. % Au obtained from CF_3AuCN^tBu was significantly less (14%), principally due to the presence of greater carbon contamination (Table 4). The EDS data also reveal that the C/Au ratios in the deposits produced by both **1a** and **1b** are very close to the C/Au ratios in the respective precursors, while the C/Au ratio in deposits produced from $Me_2Au(acac)$ is less than half of the value in the precursor. This suggests that all of the carbon atoms in the **1a** and **1b** precursors are retained in the deposits. In contrast, more than 50% of the carbon atoms in $Me_2Au(acac)$ appear to desorb during deposition, consistent with previous UHV surface science studies which have shown that CO and CH_4 are both liberated during electron irradiation of nanometer-scale films of adsorbed $Me_2Au(acac)$ molecules.[36] In addition to carbon, nitrogen is also observed in deposits created from **1a** and **1b**. Absolute nitrogen quantification was less accurate than that of carbon because of the presence of the nitrogen peak as a small shoulder on the higher energy side of the larger C K_α line. To represent the accuracy of the EDS measurements, we analyzed the compositions of the deposits shown in Figure 5 using different backgrounds and fitting protocols. Results of this analysis demonstrated that at % C and % N contents could be determined with absolute accuracies of ≈±2−3%. In contrast, the F K_α peak is almost indistinguishable from the background, despite the presence of CF_3 groups in both **1a** and **1b**.

Related experiments were also performed using X-ray photoelectron spectroscopy (XPS) to probe the effect of exposing 0.8−1.3 nm thin films of $CF_3AuCNMe$ adsorbed onto cooled (125 ± 5 K) HOPG and gold substrates to increasing doses of 500 eV electrons. Detailed spectroscopic

DOI: 10.1021/acsami.8b18368
ACS Appl. Mater. Interfaces 2019, 11, 11976−11987

analysis of the data obtained from these studies was complicated by charging that occurred within the adlayer, producing peak positions that were variable and often physically unreasonable, particularly in the Au (4f) region. However, analysis of the change in coverage of Au, C, N, and F atoms in numerous $CF_3AuCNMe$ films revealed a consistent trend, notably that electron doses on the order of 1.4×10^{18} e^-/cm^2 led to a decrease of >80% in the coverage of fluorine atoms, while the signal intensities in the C, Au, and N regions remained relatively constant (<10% change).

Both the UHV deposition experiments and the low-temperature XPS studies indicate that electron irradiation leads to the almost complete loss of fluorine in the absence of any significant carbon desorption. These results point to a process where the CF_3 ligands are subjected to sequential C−F bond cleavage events, each one accompanied by fluoride ion desorption

$$CF_{3(ads)} + e^- \rightarrow CF_{2(ads)} + F^-_{(g)}\uparrow$$

$$CF_{2(ads)} + e^- \rightarrow +e^- \rightarrow C_{(ads)} + F^-_{(g)}\uparrow$$

This reactivity trend has been observed previously in X-ray irradiation studies of semifluorinated self-assembled monolayers[63] and also explains the conversion of Teflon to amorphous carbon as a result of exposure to ionizing radiation.[64] In the context of FEBID, our results indicate that once the precursor has been decomposed into a surface-bound species, C−F bond dissociation and F desorption continue unabated as the growing deposit is continuously exposed to electron irradiation. This observation is analogous to previous studies of FEBID deposits formed from CF_3-containing precursors such as $M(hfac)_2$ (M = Pd, Pt, and Cu),[65] although the CF_3 groups in these precursors are in the ligand carbon backbone and not metal-bound.

The retention of almost all of the nitrogen and carbon atoms in both the UHV deposition experiments as well as the low-temperature XPS studies suggests that CNR ligands undergo electron-stimulated decomposition, rather than desorption, most likely initiated by electron-stimulated C−H bond cleavage.[66,67] This is in contrast to the isoelectronic CO ligands which are typically preferred "leaving groups" in organometallic precursors subject to electron irradiation.[37,44]

To further our understanding of the electron-stimulated reactions of **1a**−**b**, additional studies are underway, including (i) the effect of deposition conditions on the chemical composition of FEBID deposits and (ii) the gas-phase electron−molecule interactions of **1a**−**b**. Results from these studies will be reported in due course. Based on the results obtained in this study, it would also be interesting to study the composition of deposits created by FEBID from **2a** ClAuCNMe. Despite the lower volatility of **2a** relative to **1a** (Table 1), previous UHV surface science studies have shown that halogen atoms bonded directly to noble metals do not desorb when the precursor decomposes, but can be removed by subsequent electron irradiation.[37,44,68] This suggests that deposits generated from ClAuCNMe may have a higher gold content than both the commercial $Me_2Au(acac)$ CVD precursor and **1a**.

Relationship between MS and Deposition/UHV Experiments. It is generally well accepted that reactions of FEBID precursors are initiated by low-energy secondary electrons (energies principally <100 eV) generated by the interaction of the primary beam with the substrate.[8,69,70] Within this energy regime, two principal reaction pathways exist: dissociative electron attachment (DEA), a lower-energy process (generally <15 eV) which involves the formation and subsequent decomposition of a transient negative ion ($M + e^- \rightarrow M^- \rightarrow$ dissociation), and dissociative ionization [DI, also the process in electron impact mass spectrometry (EI-MS)], where the parent cation is formed as a precursor to potential fragmentation ($M + e^- \rightarrow M^+ + 2e^- \rightarrow$ dissociation).[69,70] Deposit formation in FEBID has been observed to proceed via DEA, DI, or a combination thereof, dependent on the individual precursor.[70] Although NCI does not perfectly mimic either process as it can consist of acid−base reactions between bath gas ions and the analyte in addition to electron transfer to the analyte, it may provide some insight into potential low-energy electron-induced dissociation reactions of FEBID precursors.

In comparing the mass spectra to the results from the deposition experiments and low-temperature XPS studies, it should be noted, however, that there are significant differences between these techniques (e.g., electron flux, gas phase vs gas-surface reactivity, precursor concentration, and sample temperature). As an example, during the steady-state depositions in the Auger spectrometer from **1a**−**b** and the UHV experiments with a few monolayers of **1a**, the results are consistent with fluorine being the only species desorbing from the surface. Loss of fluorine after ionization to form $[M - F]^+$ is also observed in the EI-MS of **1a**−**b**; however, CF_3 loss, producing $[M - CF_3]^+$, is a much more significant dissociation channel as seen in the EI-MS. We would therefore expect to observe at least some desorption of CF_3 carbons from the surface, if deposit formation in FEBID proceeded through the fragmentation pathways observed in EI-MS. Because the differences in the C/Au ratios in the deposits versus the precursors (Table 4: 2.8 vs 3 in **1a**; 5.7 vs 6 in **1b**) are small, loss of CF_3 appears to be a minor pathway if it occurs. However, the apparent lack of CF_3 desorption in the deposition experiments and low-temperature XPS studies may also be a consequence of the inability of CF_3 to desorb from the surface even if it is generated as a fragment during the decomposition of the precursor. In addition, in the MS experiments, fragments corresponding to N-dealkylation of the isocyanide are observed in the EI-MS of **1b** and in the NCI-MS of both **1a** and **1b**. To the extent that MS is predictive of the surface electron−molecule reactions, one would also expect significant loss of carbon in the deposits from dealkylation, which is not the case for the deposition conditions explored in this work. However, the composition of FEBID deposits is sensitive to the experimental conditions,[9] and the observation of these fragmentation processes in the mass spectra leaves open the possibility that analogous reactions may be encountered under other deposition conditions. Despite the differences in conditions, MS is potentially useful as a first screening tool for precursors because it illustrates possible outcomes for electron−molecule interactions in an experiment that is quick, easy, and inexpensive. Ultimately, the use of MS for prescreening of FEBID precursors is likely to be similar to the role it plays in CVD: to suggest possible precursor decomposition reactions that may or may not be major pathways under actual decomposition conditions.

CONCLUSIONS

The incentive to design new precursors for FEBID of gold nanostructures originates from stability and handling problems

DOI: 10.1021/acsami.8b18368
ACS Appl. Mater. Interfaces 2019, 11, 11976−11987

with existing Au(I) precursors in addition to the low metal content in the resulting deposits from commercial Au(III) precursors. To increase the options for Au FEBID precursors, we have designed the Au(I) precursors $CF_3AuCNMe$ (**1a**) and CF_3AuCN^tBu (**1b**). The neutral L-type isocyanide (CNR) ligands in these complexes provide stronger σ-donation into gold, adding strength to the Au−L bond. As a result, these complexes are more stable than the previously studied FEBID precursors $ClAuPF_3$ and ClAuCO. Replacement of the chloride with the trifluoromethyl (CF_3) group provides increased volatility to **1a**−**b** at 125 ± 1 mTorr with respect to the halide complexes XAuCNR (X = Cl, Br, and I; R = Me and ^{t}Bu).[34]

Precursors **1a** and **1b** were studied using MS and steady-state deposition along with low-temperature XPS studies under UHV conditions. In the preliminary screening by MS, both **1a** and **1b** showed extensive fragmentation in EI-MS with either fluorine or CF_3 loss dominating the fragmentation pattern. In NCI-MS, fragmentation is minimal. The major fragment ion observed in NCI is common to both **1a** and **1b** and corresponds to N-dealkylation of the isocyanide. The electron-induced reactions in both of the surface experiments conducted under UHV conditions (steady-state deposition and low-temperature XPS studies) are dominated by fluorine loss, with only minimal loss of the carbons from the ligands. In the steady-state deposition experiments, the deposits created from **1a**−**b** inside an AES show almost complete fluorine loss relative to the original stoichiometry of the precursors. However, the original carbon and nitrogen atoms are retained in the deposits. All three experiments agree that fluorine loss should be facile under actual FEBID conditions. Deposits made from **1a** have similar Au content to those from the commercially available $Me_2Au(acac)$ (**3**).

■ ASSOCIATED CONTENT

Supporting Information

The Supporting Information is available free of charge on the ACS Publications website at DOI: 10.1021/acsami.8b18368.

^{1}H, ^{13}C, and ^{19}F NMR spectra for complexes **1a**−**b**; TGA traces for **1a**−**b**; crystal data and structure refinement for **1a**; atomic coordinates and equivalent isotropic displacement parameters for **1a**; bond lengths and angles for **1a**; anisotropic displacement parameters for **1a**; hydrogen bonding parameters for **1a**; lattice void volume analysis for **1a** and **2a**; DIPEI and DIPNCI mass spectra for **1a**−**b**; CNR ions observed in DIPEI MS of **1b**; estimated local temperature increase during deposition; EDS and AES data from depositions using **1a** (PDF)

X-ray data for **1a** (CIF)

■ AUTHOR INFORMATION

Corresponding Author

*E-mail: lmwhite@chem.ufl.edu.

ORCID

Will G. Carden: 0000-0003-4513-6182

D. Howard Fairbrother: 0000-0003-4405-9728

Lisa McElwee-White: 0000-0001-5791-5146

Author Contributions

§R.M.T. and I.U. contributed equally to this work.

Notes

The authors declare no competing financial interest.

■ ACKNOWLEDGMENTS

L.M.-W. and D.H.F. thank the National Science Foundation for supporting this work through the linked collaborative grants CHE-1607621 and CHE-1607547. Support of preliminary studies was provided by the donors of the American Chemical Society Petroleum Research Fund (PRF grant # 54519-ND5). K.A.A. acknowledges the National Science Foundation and the University of Florida for funding the purchase of the X-ray equipment. Support of MS instrumentation was provided by the National Institute of Health through the grant S10 OD021758-01A1.

■ REFERENCES

(1) Pile, D. Perspective on Plasmonics. *Nat. Photonics* **2012**, *6*, 714.

(2) Schröter, U.; Heitmann, D. Surface-Plasmon-Enhanced Transmission Through Metallic Gratings. *Phys. Rev. B: Condens. Matter Mater. Phys.* **1998**, *58*, 15419−15421.

(3) Stockman, M. I.; Kneipp, K.; Bozhevolnyi, S. I.; Saha, S.; Dutta, A.; Ndukaife, J.; Kinsey, N.; Reddy, H.; Guler, U.; Shalaev, V. M.; Boltasseva, A.; Gholipour, B.; Krishnamoorthy, H. N. S.; MacDonald, K. F.; Soci, C.; Zheludev, N. I.; Savinov, V.; Singh, R.; Groß, P.; Lienau, C.; Vadai, M.; Solomon, M. L.; Barton, D. R.; Lawrence, M.; Dionne, J. A.; Boriskina, S. V.; Esteban, R.; Aizpurua, J.; Zhang, X.; Yang, S.; Wang, D.; Wang, W.; Odom, T. W.; Accanto, N.; de Roque, P. M.; Hancu, I. M.; Piatkowski, L.; van Hulst, N. F.; Kling, M. F. Roadmap on Plasmonics. *J. Opt.* **2018**, *20*, 043001.

(4) Lindquist, N. C.; Nagpal, P.; McPeak, K. M.; Norris, D. J.; Oh, S.-H. Engineering Metallic Nanostructures for Plasmonics and Nanophotonics. *Rep. Prog. Phys.* **2012**, *75*, 036501.

(5) Enoch, S.; Bonod, N. *Plasmonics from Basics to Advanced Topics*; Springer, 2012; Vol. *167*.

(6) McPeak, K. M.; Jayanti, S. V.; Kress, S. J. P.; Meyer, S.; Iotti, S.; Rossinelli, A.; Norris, D. J. Plasmonic Films Can Easily Be Better: Rules and Recipes. *ACS Photonics* **2015**, *2*, 326−333.

(7) Huth, M.; Porrati, F.; Schwalb, C.; Winhold, M.; Sachser, R.; Dukic, M.; Adams, J.; Fantner, G. Focused Electron Beam Induced Deposition: A Perspective. *Beilstein J. Nanotechnol.* **2012**, *3*, 597−619.

(8) van Dorp, W. F.; Hagen, C. W. A Critical Literature Review of Focused Electron Beam Induced Deposition. *J. Appl. Phys.* **2008**, *104*, 081301.

(9) Utke, I.; Hoffmann, P.; Melngailis, J. Gas-Assisted Focused Electron Beam and Ion Beam Processing and Fabrication. *J. Vac. Sci. Technol., B* **2008**, *26*, 1197.

(10) Mulders, J. J. L.; Belova, L. M.; Riazanova, A. Electron Beam Induced Deposition at Elevated Temperatures: Compositional Changes and Purity Improvement. *Nanotechnology* **2011**, *22*, 055302.

(11) Dos Santos, M. V. P.; Szkudlarek, A.; Rydosz, A.; Guerra-Nuñez, C.; Béron, F.; Pirota, K. R.; Moshkalev, S.; Diniz, J. A.; Utke, I. Comparative Study of Post-Growth Annealing of $Cu(hfac)_2$, $Co_2(CO)_8$ and $Me_2Au(acac)$ Metal Precursors Deposited by FEBID. *Beilstein J. Nanotechnol.* **2018**, *9*, 91−101.

(12) Winkler, R.; Schmidt, F.-P.; Haselmann, U.; Fowlkes, J. D.; Lewis, B. B.; Kothleitner, G.; Rack, P. D.; Plank, H. Direct-Write 3D Nanoprinting of Plasmonic Structures. *ACS Appl. Mater. Interfaces* **2017**, *9*, 8233−8240.

(13) van Dorp, W. F.; Wu, X.; Mulders, J. J. L.; Harder, S.; Rudolf, P.; De Hosson, J. T. M. Gold Complexes for Focused-Electron-Beam-Induced Deposition. *Langmuir* **2014**, *30*, 12097−12105.

(14) Shawrav, M. M.; Taus, P.; Wanzenboeck, H. D.; Schinnerl, M.; Stoger-Pollach, M.; Schwarz, S.; Steiger-Thirsfeld, A.; Bertagnolli, E. Highly Conductive and Pure Gold Nanostructures Grown by Electron Beam Induced Deposition. *Sci. Rep.* **2016**, *6*, 34003.

DOI: 10.1021/acsami.8b18368
ACS Appl. Mater. Interfaces 2019, 11, 11976−11987

(15) Folch, A. High-Vacuum Versus "Environmental" Electron Beam Deposition. *J. Vac. Sci. Technol., B: Microelectron. Nanometer Struct.–Process., Meas., Phenom.* **1996**, *14*, 2609.
(16) Jenke, M. G.; Lerose, D.; Niederberger, C.; Michler, J.; Christiansen, S.; Utke, I. Toward Local Growth of Individual Nanowires on Three-Dimensional Microstructures by Using a Minimally Invasive Catalyst Templating Method. *Nano Lett.* **2011**, *11*, 4213−4217.
(17) Höflich, K.; Yang, R. B.; Berger, A.; Leuchs, G.; Christiansen, S. The Direct Writing of Plasmonic Gold Nanostructures by Electron-Beam-Induced Deposition. *Adv. Mater.* **2011**, *23*, 2657−2661.
(18) Belić, D.; Shawrav, M. M.; Bertagnolli, E.; Wanzenboeck, H. D. Direct Writing of Gold Nanostructures with an Electron Beam: On the way to Pure Nanostructures by Combining Optimized Deposition with Oxygen-Plasma Treatment. *Beilstein J. Nanotechnol.* **2017**, *8*, 2530−2543.
(19) Botman, A.; Mulders, J. J. L.; Weemaes, R.; Mentink, S. Purification of Platinum and Gold Structures after Electron-Beam-Induced Deposition. *Nanotechnology* **2006**, *17*, 3779−3785.
(20) Utke, I.; Jenke, M. G.; Röling, C.; Thiesen, P. H.; Iakovlev, V.; Sirbu, A.; Mereuta, A.; Caliman, A.; Kapon, E. Polarisation Stabilisation of Vertical Cavity Surface Emitting Lasers by Minimally Invasive Focused Electron Beam Triggered Chemistry. *Nanoscale* **2011**, *3*, 2718−2722.
(21) Koops, H. W. P.; Kretz, J.; Rudolph, M.; Weber, M.; Dahm, G.; Lee, K. L. Characterization and Application of Materials Grown by Electron-Beam-Induced Deposition. *Jpn. J. Appl. Phys., Part 1* **1994**, *33*, 7099−7107.
(22) Huth, M.; Porrati, F.; Dobrovolskiy, O. V. Focused Electron Beam Induced Deposition Meets Materials Science. *Microelectron. Eng.* **2018**, *185*−*186*, 9−28.
(23) Graells, S.; Alcubilla, R.; Badenes, G.; Quidant, R. Growth of Plasmonic Gold Nanostructures by Electron Beam Induced Deposition. *Appl. Phys. Lett.* **2007**, *91*, 121112.
(24) Brintlinger, T.; Fuhrer, M. S.; Melngailis, J.; Utke, I.; Bret, T.; Perentes, A.; Hoffmann, P.; Abourida, M.; Doppelt, P. Electrodes for Carbon Nanotube Devices by Focused Electron Beam Induced Deposition of Gold. *J. Vac. Sci. Technol., B: Microelectron. Nanometer Struct.–Process., Meas., Phenom.* **2005**, *23*, 3174−3177.
(25) Hoffmann, P.; Utke, I.; Cicoira, F.; Dwir, B.; Leifer, K.; Kapon, E.; Doppelt, P. Focused Electron Beam Induced Deposition of Gold and Rhodium. *Mater. Res. Soc. Symp. Proc.* **2001**, *624*, 171−177.
(26) Utke, I.; Dwir, B.; Leifer, K.; Cicoira, F.; Doppelt, P.; Hoffmann, P.; Kapon, E. Electron Beam Induced Deposition of Metallic Tips and Wires for Microelectronics Applications. *Microelectron. Eng.* **2000**, *53*, 261−264.
(27) Mulders, J. J. L.; Veerhoek, J. M.; Bosch, E. G. T.; Trompenaars, P. H. F. Fabrication of Pure Gold Nanostructures by Electron Beam Induced Deposition with Au(CO)Cl Precursor: Deposition Characteristics and Primary Beam Scattering Effects. *J. Phys. D: Appl. Phys.* **2012**, *45*, 475301.
(28) Utke, I.; Hoffmann, P.; Dwir, B.; Leifer, K.; Kapon, E.; Doppelt, P. Focused Electron Beam Induced Deposition of Gold. *J. Vac. Sci. Technol., B: Microelectron. Nanometer Struct.–Process., Meas., Phenom.* **2000**, *18*, 3168−3171.
(29) Dryden, N. H.; Shapter, J. G.; Coatsworth, L. L.; Norton, P. R.; Puddephatt, R. J. [$CF_3Au(C{\equiv}NMe)$] as a Precursor for CVD of Gold. *Chem. Mater.* **1992**, *4*, 979−981.
(30) Blaya, M.; Bautista, D.; Gil-Rubio, J.; Vicente, J. Synthesis of Au(I) Trifluoromethyl Complexes. Oxidation to Au(III) and Reductive Elimination of Halotrifluoromethanes. *Organometallics* **2014**, *33*, 6358−6368.
(31) Schuster, R. E.; Scott, J. E.; Joseph Casanova, J. Methyl Isocyanide. *Org. Synth.* **2003**, *5*, 75.
(32) Heathcote, R.; Howell, J. A. S.; Jennings, N.; Cartlidge, D.; Cobden, L.; Coles, S.; Hursthouse, M. Gold(I)-Isocyanide and Gold(I)-Carbene Complexes as Substrates for the Laser Decoration of Gold onto Ceramic Surfaces. *Dalton Trans.* **2007**, 1309−1315.
(33) Martínez-Salvador, S.; Falvello, L. R.; Martín, A.; Menjón, B. Gold(I) and Gold(III) Trifluoromethyl Derivatives. *Chem.—Eur. J.* **2013**, *19*, 14540−14552.
(34) Carden, W. G.; Pedziwiatr, J.; Abboud, K. A.; McElwee-White, L. Halide Effects on the Sublimation Temperature of X−Au−L Complexes: Implications for Their Use as Precursors in Vapor Phase Deposition Methods. *ACS Appl. Mater. Interfaces* **2017**, *9*, 40998−41005.
(35) Wnuk, J. D.; Gorham, J. M.; Rosenberg, S. G.; van Dorp, W. F.; Madey, T. E.; Hagen, C. W.; Fairbrother, D. H. Electron Induced Surface Reactions of the Organometallic Precursor Trimethyl-(methylcyclopentadienyl)platinum(IV). *J. Phys. Chem. C* **2009**, *113*, 2487−2496.
(36) Wnuk, J. D.; Gorham, J. M.; Rosenberg, S. G.; van Dorp, W. F.; Madey, T. E.; Hagen, C. W.; Fairbrother, D. H. Electron Beam Irradiation of Dimethyl-(Acetylacetonate) Gold(III) Adsorbed onto Solid Substrates. *J. Appl. Phys.* **2010**, *107*, 054301.
(37) Spencer, J. A.; Wu, Y.-C.; McElwee-White, L.; Fairbrother, D. H. Electron Induced Surface Reactions of cis-$Pt(CO)_2Cl_2$: A Route to Focused Electron Beam Induced Deposition of Pure Pt Nanostructures. *J. Am. Chem. Soc.* **2016**, *138*, 9172−9182.
(38) Schödel, F.; Bolte, M.; Wagner, M.; Lerner, H.-W. Chlor-(trifluorphosphan)gold(I): [$Au(PF_3)Cl$]. *Z. Anorg. Allg. Chem.* **2006**, *632*, 652−654.
(39) Jones, P. G. The Crystal Structure of Carbonyl Gold(I) Chloride, (OC)AuCl. *Z. Naturforsch., B: J. Chem. Sci.* **1982**, *37*, 823.
(40) Dell'Amico, D.; Calderazzo, F. Convenient Methods for the Preparation of Anhydrous Gold(III) Chloride and Chlorocarbonylgold(I). *Gazz. Chim. Ital.* **1973**, *103*, 1099−1104.
(41) Tran, P. D.; Doppelt, P. Gold CVD Using Trifluorophosphine Gold(I) Chloride Precursor and its Toluene Solutions. *J. Electrochem. Soc.* **2007**, *154*, D520−D525.
(42) Cotton, F. A.; Wilkinson, G.; Murillo, C.; Bochmann, M. *Advanced Inorganic Chemistry*, 6th ed.; Wiley: New York, 1999.
(43) Fernandez, A. L.; Wilson, M. R.; Prock, A.; Giering, W. P. Evaluation of the Stereoelectronic Parameters of Fluorinated Phosphorus(III) Ligands. The Quantitative Analysis of Ligand Effects (QALE). *Organometallics* **2001**, *20*, 3429−3435.
(44) Carden, W. G.; Lu, H.; Spencer, J. A.; Fairbrother, D. H.; McElwee-White, L. Mechanism-Based Design of Precursors for Focused Electron Beam-Induced Deposition. *MRS Commun.* **2018**, *8*, 343−357.
(45) Marashdeh, A.; Tiesma, T.; van Velzen, N. J. C.; Harder, S.; Havenith, R. W. A.; De Hosson, J. T. M.; van Dorp, W. F. The Rational Design of a Au(I) Precursor for Focused Electron Beam Induced Deposition. *Beilstein J. Nanotechnol.* **2017**, *8*, 2753−2765.
(46) McElwee-White, L. Design of Precursors for the CVD of Inorganic Thin Films. *Dalton Trans.* **2006**, 5327−5333.
(47) Chen, Q.-Y. Bis(trifluoromethyl)cadmium. *Encyclopedia of Reagents for Organic Synthesis*; Wiley, 2005.
(48) Tyrra, W. E. Oxidative perfluoroorganylation methods in group 12-16 chemistry. *J. Fluorine Chem.* **2001**, *112*, 149−152.
(49) Spencer, J. A.; Rosenberg, S. G.; Barclay, M.; Wu, Y.-C.; McElwee-White, L.; Howard Fairbrother, D. Understanding the Electron-Stimulated Surface Reactions of Organometallic Complexes to Enable Design of Precursors for Electron Beam-Induced Deposition. *Appl. Phys. A* **2014**, *117*, 1631−1644.
(50) Martínez-Salvador, S.; Forniés, J.; Martín, A.; Menjón, B. [$Au(CF_3)(CO)$]: A Gold Carbonyl Compound Stabilized by a Trifluoromethyl Group. *Angew. Chem., Int. Ed.* **2011**, *50*, 6571−6574.
(51) Flörke, U.; Haupt, H. J.; Jones, P. G. Trifluoromethyl-(triphenylphosphine)gold(I). *Acta Crystallogr., Sect. C: Cryst. Struct. Commun.* **1996**, *52*, 609−611.
(52) Schneider, W.; Angermaier, K.; Sladek, A.; Schmidbaur, H. Ligand Influences on the Supramolecular Chemistry of Simple Gold(I) Complexes: Mononuclear (Isonitrile)gold(I) Complexes. *Z. Naturforsch., B: Chem. Sci.* **1996**, *51*, 790.
(53) Esperås, S.; Källson, I.; Neuvonen, K.; Keskinen, R.; Sandström, M. The Crystal and Molecular Structure of Cyano-

DOI: 10.1021/acsami.8b18368
ACS Appl. Mater. Interfaces 2019, 11, 11976−11987

(methylisocyanide)gold(I). *Acta Chem. Scand., Ser. A* **1976**, *30*, 527−530.
(54) Eggleston, D. S.; Chodosh, D. F.; Webb, R. L.; Davis, L. L. (tert-Butyl isocyanide)chlorogold(I). *Acta Crystallogr., Sect. C: Cryst. Struct. Commun.* **1986**, *42*, 36−38.
(55) Liau, R.-Y.; Mathieson, T.; Schier, A.; Berger, R. J. F.; Runeberg, N.; Schmidbaur, H. Structural, Spectroscopic and Theoretical Studies of (^{t}Butyl-isocyanide)gold(I) Iodide. *Z. Naturforsch., B: Chem. Sci.* **2002**, *57*, 881−889.
(56) White-Morris, R. L.; Olmstead, M. M.; Balch, A. L.; Elbjeirami, O.; Omary, M. A. Orange Luminescence and Structural Properties of Three Isostructural Halocyclohexylisonitrilegold(I) Complexes. *Inorg. Chem.* **2003**, *42*, 6741−6748.
(57) Hashmi, A. S. K.; Hengst, T.; Lothschütz, C.; Rominger, F. New and Easily Accessible Nitrogen Acyclic Gold(I) Carbenes: Structure and Application in the Gold-Catalyzed Phenol Synthesis as well as the Hydration of Alkynes. *Adv. Synth. Catal.* **2010**, *352*, 1315−1337.
(58) Schmidbaur, H. The Aurophilicity Phenomenon: A Decade of Experimental Findings, Theoretical Concepts and Emerging Applications. *Gold Bull.* **2000**, *33*, 3−10.
(59) Thalladi, V. R.; Weiss, H.-C.; Bläser, D.; Boese, R.; Nangia, A.; Desiraju, G. R. C−H···F Interactions in the Crystal Structures of Some Fluorobenzenes. *J. Am. Chem. Soc.* **1998**, *120*, 8702−8710.
(60) Pitts, C. R.; Siegler, M. A.; Lectka, T. Intermolecular Aliphatic C−F···H−C Interaction in the Presence of "Stronger" Hydrogen Bond Acceptors: Crystallographic, Computational, and IR Studies. *J. Org. Chem.* **2017**, *82*, 3996−4000.
(61) Shimoni, L.; Glusker, J. P. The geometry of intermolecular interactions in some crystalline fluorine-containing organic compounds. *Struct. Chem.* **1994**, *5*, 383−397.
(62) McClain, K. R.; O'Donohue, C.; Koley, A.; Bonsu, R. O.; Abboud, K. A.; Revelli, J. C.; Anderson, T. J.; McElwee-White, L. Tungsten Nitrido Complexes as Precursors for Low Temperature Chemical Vapor Deposition of WN_xC_y Films as Diffusion Barriers for Cu Metallization. *J. Am. Chem. Soc.* **2014**, *136*, 1650−1662.
(63) Perry, C. C.; Wagner, A. J.; Fairbrother, D. H. Electron Stimulated C-F Bond Breaking Kinetics in Fluorine-Containing Organic Thin Films. *Chem. Phys.* **2002**, *280*, 111−118.
(64) Wheeler, D. R.; Pepper, S. V. X-Ray Photoelectron and Mass Spectroscopic Study of Electron Irradiation and Thermal Stability of Polytetrafluoroethylene. *J. Vac. Sci. Technol., A* **1990**, *8*, 4046−4056.
(65) Rosenberg, S. G.; Barclay, M.; Fairbrother, D. H. Electron Induced Surface Reactions of Organometallic Metal(hfac)$_2$ Precursors and Deposit Purification. *ACS Appl. Mater. Interfaces* **2014**, *6*, 8590−8601.
(66) Huels, M. A.; Dugal, P.-C.; Sanche, L. Degradation of Functionalized Alkanethiolate Monolayers by 0-18 eV Electrons. *J. Chem. Phys.* **2003**, *118*, 11168−11178.
(67) Rowntree, P. A. The Use of Highly Organized Molecular Films as Electron Scattering Targets: Spectroscopic and Desorption Measurements of Selective Bond Rupture in Organic Films. *Surf. Sci.* **1997**, *390*, 70−78.
(68) Spencer, J. A.; Brannaka, J. A.; Barclay, M.; McElwee-White, L.; Fairbrother, D. H. Electron-Induced Surface Reactions of η^3-Allyl Ruthenium Tricarbonyl Bromide [$(\eta^3$-$C_3H_5)$Ru$(CO)_3$Br]: Contrasting the Behavior of Different Ligands. *J. Phys. Chem. C* **2015**, *119*, 15349−15359.
(69) Böhler, E.; Warneke, J.; Swiderek, P. Control of Chemical Reactions and Synthesis by Low-Energy Electrons. *Chem. Soc. Rev.* **2013**, *42*, 9219−9231.
(70) Thorman, R. M.; Kumar, T. P. R.; Fairbrother, D. H.; Ingólfsson, O. The Role of Low-Energy Electrons in Focused Electron Beam Induced Deposition: Four Case Studies of Representative Precursors. *Beilstein J. Nanotechnol.* **2015**, *6*, 1904−1926.

DOI: 10.1021/acsami.8b18368
ACS Appl. Mater. Interfaces 2019, 11, 11976−11987